Dissipative finite element formulation applied to piezoelectric materials with Debye memory

Roberto Palma[1], J.L. Pérez-Aparicio[2], Robert L. Taylor[3]
[1]Department of Mechanical Engineering and Construction, Universitat Jaume I, Spain
[2]Department of Continuum Mechanics and Theory of Structures, Universitat Politècnica de València, Spain
[3]Department of Civil and Environmental Engineering, University of California at Berkeley, California, USA

This work presents a finite element study of the Debye memory in piezoelectric devices. This memory dependency is due to the spontaneous polarization of the electric dipoles and it can be understood as a transient viscosity-like effect. The formulation assumes a small strain and rotation hypothesis and the main contribution is the inclusion of time-dependent constitutive behavior. For this purpose, a unique numerical formulation that uses convolution integrals is developed to solve the time-dependent electric constitutive equation. A consistent and monolithic finite element formulation is then obtained and implemented. Finally, a commercial piezoelectric device is simulated for two operational modes: an actuator and a sensor. Several important conclusions on the coupled mechanical and electric fields are reported and the stability of the time integration scheme is tested by representing the time evolution of the electro-mechanic energy.

I. Introduction

Piezoelectric materials are widely used in mechatronic devices [**?**], [**?**], [**?**] due to their intrinsic ability to couple electric and mechanic energies. Consequently, these materials are commonly incorporated in sensors, actuators, ultrasonic transducers, smart structures, energy harvesters, medical devices, etc. There is then an increasing need for cutting-edge simulation tools to study and optimize current and future development of sophisticated industrial equipment.

As in many scientific and technological fields, piezoelectric studies started from the necessity of develop practical devices: the initial emphasis in the decade of 1960 was in applicability [**?**]. While the electrical and mechanical basics were rapidly understood, more advanced issues (e.g. numerical solutions, nonlinearities) were dealt with in the 1990s [**?**]. From a mechanical point of view piezoelectric devices have been extensively studied for both small and large strains. For the former, the authors of the present work have published several articles using finite element methods (FE): [**?**], [**?**], [**?**], [**?**] and [**?**]. For the latter, polyconvex approaches are reported in [**?**]. Other numerical techniques such as the boundary element method have been applied to model small strain piezoelectrics, see [**?**].

In contrast to advances in the mechanical behavior, some electrical behavior has not yet been completely simulated. One of these is the Debye effect, also called Debye memory: see the classical [**?**] and the recents [**?**], [**?**]. The Debye effect can be understood as a dielectric relaxation similar to viscoelasticity in continuum mechanics. This memory incorporates irreversibilities due to delays in microscopic polarizations that can be relevant for high-frequency applications such as ultrasonics.

In the present work a three-dimensional, pseudo non-linear, transient numerical formulation based on the FE method is developed to model piezoelectric materials with Debye memory. The governing equations are obtained from the Extended Non-Equilibrium Thermodynamics (ENET) [**?**], and discretized with standard isoparametric shape functions. Although the governing equations are linear, the results present loop shapes because of the strong dissipation induced by the memory. A Newmark-β algorithm [**?**] is used to discretize inertial effects and is combined with convolution integrals to solve the irreversibility from Debye terms.

The resulting formulation is implemented into the research FE code `FEAP` [**?**] and several examples are presented to highlight the importance of the Debye effect in piezoelectric applications. A piezoelectric plate is simulated and polarization evolutions for several prescribed shapes (steps and spikes) and frequencies of the electric field are shown.

A limitation of the presented model is the consideration of the mechanical field as linear and elastic, although the material is studied as transversely isotropic. Another restriction is the absence of magnetic field, that is the objective of an ongoing research [**?**]. Thermal effects are also ignored and will be studied in the future since under high frequencies some piezoelectric devices tend to overheat.

II. Governing equations

The governing equations for the piezoelectric problem with Debye memory are balance of linear and angular momentum, Gauss law from Maxwell's equations, constitutive equations and initial and boundary conditions. Constitutive equations are obtained from an electromagnetic enthalpy that couples both mechanical and electrical energies. Irreversibilities appear due to the presence of the Debye effect; consequently, the constitutive equations are expressed as the sum of reversible terms, as in classical piezoelectricity, and irreversible terms, as for Debye memory.

A. Equilibrium equations

Consider a domain Ω and boundary Γ with outward normal $\mathbf{n}$, see Fig. **??**. The local balance of momentum of a mechan-

Manuscript received –, 2017; revised –, 2017. Corresponding author: R. Palma (email: rpalma@uji.es).

ical system is given by:

$$\rho_m \; \ddot{\boldsymbol{u}} = \nabla \cdot \boldsymbol{T} + \boldsymbol{f}, \tag{1}$$

where ρ_m, $\boldsymbol{u}$ and $\boldsymbol{T}$ denote mass density, displacement vector, Cauchy stress tensor and body force, respectively. The symbols $(\dot{\ })$, ∇ and $(\cdot)$ are used for time derivation, Del operator and dot product, respectively. The body forces are included in $\boldsymbol{f}$; in common applications they are gravity, external fields, etc.

Balance of angular momentum is automatically satisfied by the symmetry of $\boldsymbol{T}$.

Assuming small strains, displacements and rotations, the strain tensor is obtained as the symmetric part of the displacement gradient; in the present work it is expressed by:

$$\boldsymbol{S} = \frac{1}{2}\Big(\nabla \otimes \boldsymbol{u} + \boldsymbol{u} \otimes \nabla\Big) \doteq \nabla^{sy}\boldsymbol{u}, \tag{2}$$

where $\otimes$ is the outer product.

For electrical equilibrium, the Gauss law is introduced as:

$$\nabla \cdot \boldsymbol{D} = \rho_q, \tag{3}$$

where $\boldsymbol{D}$ denotes electric displacement and ρ_q the volumetric electric charge density. Using now the two electric Maxwell equations in absence of a magnetic field and the Helmholtz decomposition theorem (also called fundamental theorem of vector calculus), the electric field $\boldsymbol{E}$ is obtained from a scalar electric potential for voltage V:

$$\boldsymbol{E} = -\nabla V. \tag{4}$$

B. Polarization vector

In electromagnetism [**?**], the polarization vector $\boldsymbol{P}$ typically expresses the density of permanent or induced electric dipole moments in a dielectric material. The Fig. **??** represents a piezoelectric domain with a wide range of randomly oriented dipoles. Macroscopically and in the presence of Debye memory, $\boldsymbol{P}$ is composed of two microscopic terms:

$$\boldsymbol{P} = \sum_i \Big[\boldsymbol{p}_i^0 - \boldsymbol{p}_i(t)\Big]. \tag{5}$$

On the one hand, $\boldsymbol{p}^0$ represents the instantaneous polarization of each dipole moment and it is directly related with reversible processes as in classical piezoelectric theory. On the other hand, $\boldsymbol{p}(t)$ represents the momentary delay in polarizable media, and it is responsible for the Debye memory that introduces irreversibilities with entropy production.

From a macroscopic point of view and according to the ENET, see [**?**], [**?**], this irreversibility is taken into account by the introduction of an empirical relaxation time τ_P. Consequently, (**??**) is expressed as the sum of reversible and irreversible terms. In addition and as common in electromagnetism, the polarization is substituted with the electric displacement vector, again divided into reversible $\boldsymbol{D}_r$ and irreversible $\tau_P\dot{\boldsymbol{D}}$ terms:

$$\boldsymbol{D} \doteq \underbrace{\boldsymbol{D}_r}_{\text{rev.}} - \underbrace{\tau_P\dot{\boldsymbol{D}}}_{\text{irrev.}}, \tag{6}$$

where the second term of the right side is dimensionally correct.

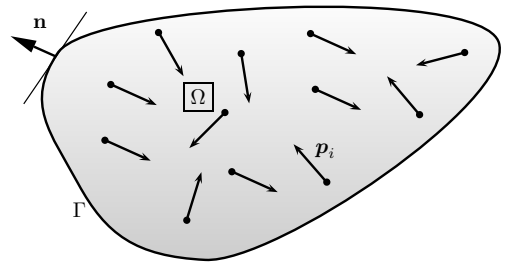

Fig. 1. A piezoelectric of domain Ω and boundary Γ with outward normal $\mathbf{n}$ and with randomly oriented electric dipoles $\boldsymbol{p}_i$.

C. Constitutive equations

These equations are obtained from thermodynamic energy potentials and relate cause and effect variables. In the present work, these equations firstly relate mechanical tensors—$\boldsymbol{T}$ with $\boldsymbol{S}$—and secondly electrical fields—$\boldsymbol{D}$ with $\boldsymbol{E}$.

For an amenable FE implementation based on displacements (mechanical $\boldsymbol{u}$ and voltage V), the electromagnetic enthalpy potential $\Pi(\boldsymbol{S}, \boldsymbol{E}, \dot{\boldsymbol{D}}) = \Pi^r(\boldsymbol{S}, \boldsymbol{E}) + \Pi^i(\dot{\boldsymbol{D}})$ is set applying a Legendre transformation to the total internal energy $U = U(\boldsymbol{S}, \boldsymbol{D}_r, \dot{\boldsymbol{D}})$. Π^r denotes the reversible energy that is exchanged between mechanic and electric fields and $\Pi^i = \tau_P \boldsymbol{E} \cdot \dot{\boldsymbol{D}}$ is the irreversible electric energy (also called non-conservative or damping effect) that is converted into heat due to the Debye memory. Other irreversibilities which increase temperature could be added—for instance Biot terms—but they are not the aim of the current work.

The objective of the Legendre transformation is to replace $\boldsymbol{D}_r$ by $\boldsymbol{E}$ to take advantage of the "kinematic" variables (using the mechanical nomenclature) (**??**) and (**??**).

In a first and qualified approximation, Π can be obtained by applying to $\Pi(\boldsymbol{S}, \boldsymbol{E}, \dot{\boldsymbol{D}})$ a Taylor series expansion considering only terms up to quadratic degree:

$$\Pi(\boldsymbol{S}, \boldsymbol{E}, \dot{\boldsymbol{D}}) = \frac{1}{2}\Big(\boldsymbol{S} : \mathbf{C} : \boldsymbol{S} - \boldsymbol{E} \cdot \boldsymbol{\epsilon} \cdot \boldsymbol{E}\Big) - \boldsymbol{e}^V : \boldsymbol{S} \cdot \boldsymbol{E} + \tau_P \boldsymbol{E} \cdot \dot{\boldsymbol{D}}, \tag{7}$$

where $\mathbf{C}$ denotes a fourth order tensor of elastic moduli, $\boldsymbol{\epsilon}$ is a second order permittivity tensor and $\boldsymbol{e}^V$ is a third order piezoelectric tensor. In addition, the symbol $(:)$ denotes double contraction (also called double dot product) of the contiguous tensors. Generally, in finite element development of elastic bodies second order tensors are replaced by vectors using Voigt notation [**?**]. Thus, third and fourth order tensors become matrices where the stress and strain indices are mapped according to:

$$\begin{aligned} S_{ij} \;&\rightarrow\; \begin{bmatrix} S_{11} & S_{22} & S_{33} & 2\,S_{12} & 2\,S_{23} & 2\,S_{31} \end{bmatrix}, \\ T_{ij} \;&\rightarrow\; \begin{bmatrix} T_{11} & T_{22} & T_{33} & T_{12} & T_{23} & T_{31} \end{bmatrix}. \end{aligned} \tag{8}$$

Finally, the constitutive equations are obtained by differentiation of Π from (**??**) with respect to $\boldsymbol{S}$ and $\boldsymbol{E}$. Taking into account (**??**) this yields:

$$\begin{aligned} \boldsymbol{T} \;&=\; \frac{\partial \Pi}{\partial \boldsymbol{S}} \;= \mathbf{C} : \boldsymbol{S} - (\boldsymbol{e}^V)^\top \cdot \boldsymbol{E}, \\ \boldsymbol{D} \;&=\; -\frac{\partial \Pi}{\partial \boldsymbol{E}} \;= \boldsymbol{\epsilon} \cdot \boldsymbol{E} + \boldsymbol{e}^V : \boldsymbol{S} - \tau_P \dot{\boldsymbol{D}}, \end{aligned} \tag{9}$$

where the supraindex $(\ )^\top$ denotes transposition of a vector or a matrix.

D. Boundary conditions

The coupled equations given by (**??**), (**??**), (**??**), (**??**) and (**??**) require satisfaction of boundary conditions. Here, two simple types of Dirichlet and Neumann conditions are used. Since the problem is coupled, both boundary conditions are composed of mechanical and electrical terms, given by:

$$\begin{array}{cc} \underline{\text{Dirichlet type}} & \underline{\text{Neumann type}} \\ \boldsymbol{u} = \overline{\boldsymbol{u}}, & \boldsymbol{T}\cdot\mathbf{n} = \overline{\boldsymbol{t}}, \\ V = \overline{V}, & \boldsymbol{D}\cdot\mathbf{n} = \overline{q}_\Gamma, \end{array} \tag{10}$$

where $\overline{\boldsymbol{u}}$, $\overline{V}$, $\overline{\boldsymbol{t}}$ and $\overline{q}_\Gamma$ denote prescribed displacements, prescribed voltage, traction vector, and electric charges on Γ, respectively. This boundary must be split in two parts for both types of boundary conditions: Γ_D and Γ_N.

E. Initial conditions

The momentum equation requires initial conditions for displacement and velocity and, due to the Debye effect, the electric displacement also requires an initial value.

$$\boldsymbol{u}(0) = \bar{\boldsymbol{u}}^0, \qquad \dot{\boldsymbol{u}}(0) = \bar{\dot{\boldsymbol{u}}}^0, \qquad \boldsymbol{D}(0) = \bar{\boldsymbol{D}}^0. \tag{11}$$

Zero values are assumed for all of them in this work.

III. Finite element formulation

This section presents a numerical discretization, based on the FE method, of the governing equations reported in Sec. **??**.

A. Weak forms

The governing equations are expressed in strong forms, namely, they are 2nd order differential functions of the degrees of freedom $\boldsymbol{u}$ and V. For an amenable FE formulation, the weak forms must be calculated following the steps:

- (**??**) and (**??**) are multiplied by arbitrary test functions denoted by $\delta\boldsymbol{u}$ and δV.
- the divergence theorem is applied to the gradient terms of both equations.
- the Neumann boundary conditions (**??**) are enforced with a boundary integral Γ_N.

The resulting weak forms are given by:

$$\begin{aligned} \int_\Omega \Big[\delta\boldsymbol{u}\cdot(\boldsymbol{f} - \rho_m\ddot{\boldsymbol{u}}) - \delta\boldsymbol{S}:\boldsymbol{T}\Big]\ \mathrm{d}\Omega + \oint_{\Gamma_N} \delta\boldsymbol{u}\cdot\bar{\boldsymbol{t}}\ \mathrm{d}\Gamma &= 0, \\ \int_\Omega \Big[\delta V\rho_q + (\nabla\delta V)\cdot\boldsymbol{D}\Big]\ \mathrm{d}\Omega - \oint_{\Gamma_N} \delta V\ \bar{q}_\Gamma\ \mathrm{d}\Gamma &= 0. \end{aligned} \tag{12}$$

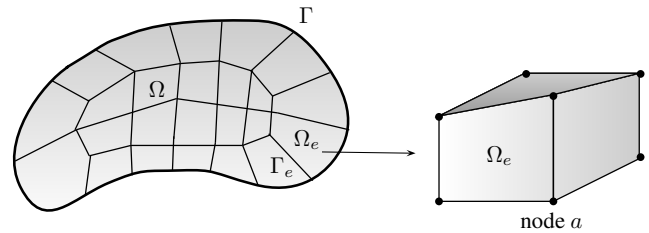

Fig. 2. A continuum domain Ω with boundary Γ is discretized with n three-dimensional eight-node brick elements of domain Ω_e and boundary Γ_e.

B. Discretizations: Convolution integrals

The continuum domain is discretized by n three-dimensional eight-node brick elements of domain Ω_e and boundary Γ_e such that $\Omega \approx \sum_i^n \Omega_e$ (see Fig. **??**). Standard shape functions $\mathcal{N}$ are expressed as a function of parametric coordinates $\boldsymbol{\xi}$ for each element. An isoparametric interpolation is adopted such that global cartesian coordinates $\boldsymbol{x}$, degrees of freedom and test functions are approximated by the same $\mathcal{N}$:
.

$$\begin{aligned} &\boldsymbol{x} \approx \mathcal{N}_a\ \tilde{\boldsymbol{x}}_a\ , \\ &\boldsymbol{u} \approx \mathcal{N}_a\ \tilde{\boldsymbol{u}}_a\ , \quad \ddot{\boldsymbol{u}} \approx \mathcal{N}_a\ \tilde{\ddot{\boldsymbol{u}}}_a\ , \quad \delta\boldsymbol{u} \approx \mathcal{N}_a\ \delta\tilde{\boldsymbol{u}}_a\ , \\ &V \approx \mathcal{N}_a\ \tilde{V}_a\ , \quad \delta V \approx \mathcal{N}_a\ \delta\tilde{V}_a, \end{aligned} \tag{13}$$

where $\tilde{\boldsymbol{x}}_a$, $\tilde{\boldsymbol{u}}_a$, $\tilde{V}_a$ denote a nodal value at the local node a (or alternatively b) of the mesh, and summation for repeated indices a or b is applied. Likewise, (**??**) and (**??**) are approximated by:

$$\begin{aligned} \boldsymbol{S} &\approx \nabla^{sy}\mathcal{N}_a\ \tilde{\boldsymbol{u}}_a &&= \boldsymbol{\mathcal{B}}_a^{sy}\ \tilde{\boldsymbol{u}}_a, \\ \boldsymbol{E} &\approx -\nabla\mathcal{N}_a\ \tilde{V}_a &&= -\boldsymbol{\mathcal{B}}_a\ \tilde{V}_a, \end{aligned} \tag{14}$$

$$\boldsymbol{\mathcal{B}}_a^{sy} = \begin{bmatrix} \mathcal{N}_{a,1} & 0 & 0 \\ 0 & \mathcal{N}_{a,2} & 0 \\ 0 & 0 & \mathcal{N}_{a,3} \\ \mathcal{N}_{a,2} & \mathcal{N}_{a,1} & 0 \\ 0 & \mathcal{N}_{a,3} & \mathcal{N}_{a,2} \\ \mathcal{N}_{a,3} & 0 & \mathcal{N}_{a,1} \end{bmatrix}, \qquad \boldsymbol{\mathcal{B}}_a = \begin{Bmatrix} \mathcal{N}_{a,1} \\ \mathcal{N}_{a,2} \\ \mathcal{N}_{a,3} \end{Bmatrix}, \tag{15}$$

where $(\cdot_{,j})$ denotes differentiation with respect to the jth Cartesian coordinate.

Time discretization of the momentum equation is performed using the Newmark method given by:

$$\begin{aligned} \tilde{\boldsymbol{u}}_a^{n+1} &= \tilde{\boldsymbol{u}}_a^n + \Delta t\ \tilde{\dot{\boldsymbol{u}}}_a^n + \Delta t^2\Big[\big(\tfrac{1}{2} - \beta_N\big)\ \tilde{\ddot{\boldsymbol{u}}}_a^n + \beta_N\tilde{\ddot{\boldsymbol{u}}}_a^{n+1}\Big], \\ \tilde{\dot{\boldsymbol{u}}}_a^{n+1} &= \tilde{\dot{\boldsymbol{u}}}_a^n + \Delta t\ \Big[\big(1 - \gamma_N\big)\ \tilde{\ddot{\boldsymbol{u}}}_a^n + \gamma_N\ \tilde{\ddot{\boldsymbol{u}}}_a^{n+1}\Big], \end{aligned} \tag{16}$$

where $\tilde{\boldsymbol{u}}_a^n$, $\tilde{\dot{\boldsymbol{u}}}_a^n$, $\tilde{\ddot{\boldsymbol{u}}}_a^n$ are approximate values of nodal displacement, velocity and acceleration at time t_n, respectively, and β_N and γ_N are parameters to control stability and accuracy. The time increment is denoted by $\Delta t = t_{n+1} - t_n$, where $n+1$ represents the current and n the previous time steps.

The discretized form of the mechanical constitutive (**??**) is directly calculated by means of (**??**) to give:

$$\boldsymbol{T}^{n+1} \approx \mathbf{C}\ \boldsymbol{\mathcal{B}}_a^{sy}\ \tilde{\boldsymbol{u}}_a^{n+1} + (\boldsymbol{e}^V)^\top\ \boldsymbol{\mathcal{B}}_a\ \tilde{V}_a^{n+1}. \tag{17}$$

Due to the presence of the Debye memory, the electric constitutive (**??**) is an ordinary differential equation; for constant material properties an exact solution to the differential equation may be computed from the solution to the homogeneous equation using variation of parameters:

$$\begin{aligned}\boldsymbol{D}(t) &= \bar{\boldsymbol{D}}^0\ \mathrm{e}^{-t/\tau_P} \\ &+ \frac{1}{\tau_P}\int_0^t \Big[\boldsymbol{e}^V : \boldsymbol{S}(t') + \boldsymbol{\epsilon}\cdot\boldsymbol{E}(t')\Big]\ \mathrm{e}^{-(t-t')/\tau_P}\ \mathrm{d}t',\end{aligned} \tag{18}$$

where $\bar{\boldsymbol{D}}^0$ is determined from (**??**). Evaluating (**??**) at t_n and t_{n+1} leads to the incremental form:

$$\begin{aligned}\boldsymbol{D}^{n+1} &= \mathrm{e}^{-\Delta t/\tau_P}\,\boldsymbol{D}^n \\ &+ \frac{1}{\tau_P}\int_{t_n}^{t_{n+1}} \Big[\boldsymbol{e}^V : \boldsymbol{S}(t') + \boldsymbol{\epsilon}\cdot\boldsymbol{E}(t')\Big]\ \mathrm{e}^{-(t_{n+1}-t')/\tau_P}\ \mathrm{d}t'.\end{aligned} \tag{19}$$

The time evolution of $\boldsymbol{S}(t')$ and $\boldsymbol{E}(t')$ may be approximated at each time increment by the finite difference θ-method [**?**]:

$$\begin{aligned}\boldsymbol{S}(t') &\approx (1-\theta_1)\ \boldsymbol{S}_n + \theta_1\ \boldsymbol{S}_{n+1}, \\ \boldsymbol{E}(t') &\approx (1-\theta_2)\ \boldsymbol{E}_n + \theta_2\ \boldsymbol{E}_{n+1},\end{aligned} \tag{20}$$

which includes both the explicit Euler $\theta_1 = \theta_2 = 0$ and the implicit Crank-Nicolson $\theta_1 = \theta_2 = 1/2$ methods. Introducing (**??**) into (**??**) yields:

$$\begin{aligned}\boldsymbol{D}^{n+1} &= \mathrm{e}^{-\Delta t/\tau_P}\boldsymbol{D}^n + \Big\{\boldsymbol{e}^V\big[(1-\theta_1)\ \boldsymbol{S}^n + \theta_1\ \boldsymbol{S}^{n+1}\big] \\ &+ \boldsymbol{\epsilon}\ \big[(1-\theta_2)\ \boldsymbol{E}^n + \theta_2\ \boldsymbol{E}^{n+1}\big]\Big\}\Big(1-\mathrm{e}^{-\Delta t/\tau_P}\Big),\end{aligned} \tag{21}$$

where the integral of the exponential term was solved as:

$$\frac{1}{\tau_P}\int_{t_n}^{t_{n+1}} \mathrm{e}^{-(t_{n+1}-t')/\tau_P}\ \mathrm{d}t' = 1 - \mathrm{e}^{-\Delta t/\tau_P}. \tag{22}$$

The memory and coupled effects are represented by the dependency of both mechanical and electrical degrees of freedom on the current and previous time steps.

C. Residuals and tangent matrices

Although the present problem is linear, the FE formulation is based on mechanical and electric residuals $\boldsymbol{\mathcal{R}}^u$ and $\mathcal{R}^V$ to accommodate future non-linear developments. For instance, induced electrostriction or dependency of material properties with basic variables will be studied in the future. Therefore, the approximated solutions are achieved by minimizing these residuals with the Newton-Raphson algorithm, [**?**]. Mathematically, residuals are calculated introducing the discretizations (**??**), (**??**) into the weak forms (**??**):

$$\begin{aligned}\boldsymbol{\mathcal{R}}_a^{u,n+1} &= \int_{\Omega_e}\Big[\boldsymbol{\mathcal{B}}_a^{sy\top}\ \boldsymbol{T}^{n+1} + \mathcal{N}_a\big(\boldsymbol{f} - \rho_m\ \mathcal{N}_b\ \tilde{\ddot{\boldsymbol{u}}}_b^{n+1}\big)\Big]\ \mathrm{d}\Omega_e \\ &+ \oint_{\Gamma_e} \mathcal{N}_a\ \bar{\boldsymbol{t}}\ \mathrm{d}\Gamma_e, \\ \mathcal{R}_a^{V,n+1} &= \int_{\Omega_e}\Big(\boldsymbol{B}_a^\top\ \boldsymbol{D}^{n+1} + \mathcal{N}_a\ \rho_q\Big)\ \mathrm{d}\Omega_e \\ &- \oint_{\Gamma_e} \mathcal{N}_a\ \bar{q}_\Gamma\ \mathrm{d}\Gamma_e.\end{aligned} \tag{23}$$

The present FE formulation is based on a monolithic approach, that is, fully coupled tangent stiffness matrices are calculated.

To develop these tangent matrices for the Newton solution, a linearization of the residuals with respect to the degrees of freedom $\tilde{\boldsymbol{u}}_b^{n+1}$ and $\tilde{V}_b^{n+1}$ is performed. The element matrices are assembled in a standard FE scheme to form the total matrices for the problem. The resulting system yields:

$$\begin{bmatrix}\boldsymbol{\mathcal{K}}_{ab}^{uu} + c_3\ \boldsymbol{\mathcal{M}}_{ab}^{uu} & \boldsymbol{\mathcal{K}}_{ab}^{uV} \\ \boldsymbol{\mathcal{K}}_{ab}^{Vu} & \mathcal{K}_{ab}^{VV}\end{bmatrix}^k \begin{Bmatrix}\mathrm{d}\tilde{\boldsymbol{u}}_b^{n+1} \\ \mathrm{d}\tilde{V}_b^{n+1}\end{Bmatrix}^k = \begin{Bmatrix}\boldsymbol{\mathcal{R}}_a^{u,n+1} \\ \mathcal{R}_a^{V,n+1}\end{Bmatrix}^k, \tag{24}$$

where $\boldsymbol{\mathcal{K}}$ and $\boldsymbol{\mathcal{M}}$ denote tangent stiffness and mass matrices, and c_3 results from linearizing the Newmark relations (**??**) to give:

$$\mathrm{d}\tilde{\boldsymbol{u}}_a^{n+1} = \beta_N\ \Delta t^2\ \mathrm{d}\tilde{\ddot{\boldsymbol{u}}}_a^{n+1} \quad \rightarrow \quad c_3 = \frac{1}{\beta_N \Delta t^2}. \tag{25}$$

These matrices are obtained by derivation of (**??**); only the terms that explicitly depend on the degrees of freedom remain:

$$\begin{aligned}\boldsymbol{\mathcal{K}}_{ab}^{uu} &= \int_{\Omega_e} \boldsymbol{\mathcal{B}}_a^{sy\top}\ \frac{\partial \boldsymbol{T}^{n+1}}{\partial \tilde{\boldsymbol{u}}_b^{n+1}}\ \mathrm{d}\Omega_e, \\ \boldsymbol{\mathcal{K}}_{ab}^{uV} &= \int_{\Omega_e} \boldsymbol{\mathcal{B}}_a^{sy\top}\ \frac{\partial \boldsymbol{T}^{n+1}}{\partial \tilde{V}_b^{n+1}}\ \mathrm{d}\Omega_e, \\ \boldsymbol{\mathcal{K}}_{ab}^{Vu} &= -\int_{\Omega_e} \boldsymbol{\mathcal{B}}_a^{\top}\ \frac{\partial \boldsymbol{D}^{n+1}}{\partial \tilde{\boldsymbol{u}}_b^{n+1}}\ \mathrm{d}\Omega_e, \\ \mathcal{K}_{ab}^{VV} &= -\int_{\Omega_e} \boldsymbol{\mathcal{B}}_a^{\top}\ \frac{\partial \boldsymbol{D}^{n+1}}{\partial \tilde{V}_b^{n+1}}\ \mathrm{d}\Omega_e, \\ \boldsymbol{\mathcal{M}}_{ab}^{uu} &= \int_{\Omega_e} \mathcal{N}_a\ \rho_m\ \boldsymbol{I}\ \mathcal{N}_b\ \mathrm{d}\Omega_e,\end{aligned} \tag{26}$$

where $\boldsymbol{I}$ is the identity second order tensor. The previous derivatives are explicitly calculated using (**??**) and (**??**):

$$
\begin{aligned}
\frac{\partial \boldsymbol{T}^{n+1}}{\partial \tilde{\boldsymbol{u}}_b^{n+1}} &= \mathbf{C}\ \boldsymbol{\mathcal{B}}_b^{sy}, \qquad \frac{\partial \boldsymbol{T}^{n+1}}{\partial \tilde{V}_b^{n+1}} = (\boldsymbol{e}^V)^\top\ \boldsymbol{\mathcal{B}}_b, \\
\frac{\partial \boldsymbol{D}^{n+1}}{\partial \tilde{\boldsymbol{u}}_b^{n+1}} &= \theta_1 \left(1 - \mathrm{e}^{-\Delta t/\tau_P}\right) \boldsymbol{e}^V\ \boldsymbol{\mathcal{B}}_b^{sy}, \\
\frac{\partial \boldsymbol{D}^{n+1}}{\partial \tilde{V}_b^{n+1}} &= -\theta_2 \left(1 - \mathrm{e}^{-\Delta t/\tau_P}\right) \boldsymbol{\epsilon}\ \boldsymbol{\mathcal{B}}_b.
\end{aligned} \tag{27}
$$

The time-dependency appears only in the last two equations.

This FE formulation is implemented in the FE system `FEAP` [**?**]. The main advantage of this system are that the required solvers are already developed and users only have to implement their formulations into a user element.

IV. Results

This section reports several numerical results to study the influence of the Debye memory on the response of piezoelectric devices. For this purpose, a rectangular piezoelectric plate 7R-34-23-2500 made out of P-5E (lead zirconate titanate) and manufactured by `Piezotite` [**?**] is studied. The dimensions are $33.3 \times 22.8 \times 0.8$ (mm), see Fig. **??**, the polarization is along the thickness and the material properties given in Table **??**.

This piezoelectric is recommended for ultrasonic actuator applications and its maximum allowable voltage is $V_{mx} = 0.7E_c h = 840$ (V), where $E_c = 1.5\times10^6$ (V/m) is the coercive field and h the plate thickness.

Although constructed for the actuator mode, this device can also be employed in the sensor mode. In the former, an electric field is prescribed by a time-dependent voltage and a mechanical vibration is caused; in the latter, a mechanical vibration caused by a time-dependent vertical displacement $w(t)$ induces an electric field. The second mode is the basis of energy harvesters and/or frequency monitoring of strains/displacements. The other boundary conditions for both modes are shown in Fig. **??**: mechanically, they are fixed-free and electrically the voltage is set to zero at the bottom.

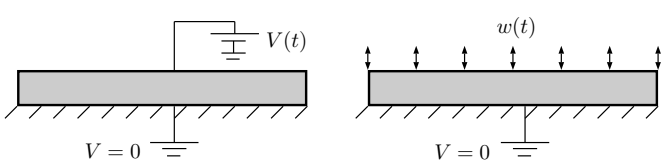

Fig. 3. Front view of the piezoelectric plate and sketches of both mode operations: actuator with time-dependent voltage (left) and sensor with vertical displacement (right).

For studying the response of piezoelectrics with memory, the relaxation parameters τ_P can be approximately calculated by the Casimir limit defined in [**?**] and modified by [**?**]. In the second reference, the original limit based on temperature T is converted into another based on polarization. Notice that τ_P depends on the application velocity of the electric and mechanic fields and on the material; τ_P is very small with $O(10^{-9})$ for polymers, colloids and glassy systems and relatively large for ceramics at the macro scale with $O(10^{-1})$; see [**?**] for both orders of magnitude.

Three relaxations are considered here: τ_P = 0, 10, 80 (s); the zero value corresponds to the classical piezoelectricity (without memory) and it is included for comparisons with the others. The previous values of τ_P are based on [**?**], where an estimation of $\tau_P = 1$ (s) is assumed with $\epsilon \approx 5\epsilon_0$. For `Piezotite`, $\epsilon \approx 960\epsilon_0$ and, consequently, the value 80 (s) seems reasonable.

From the numerical point of view, the piezoelectric device is modeled by using 200 eight-node, three-dimensional elements with eight integration points, see Fig. **??**. For all simulations, parameters θ_1 = θ_2 = 1/2 are chosen, resulting in an implicit scheme that facilitates the integration of the time-dependent electric constitutive (**??**). This implicitness is also coherent with the use of the standard Newmark-β with $\beta_N = 1/4$ for the time integration with $\Delta t = 0.5$ (s) of the hyperbolic mechanical expression (**??**). Finally, the variables $\boldsymbol{S}$ and $\boldsymbol{E}$ are numerically obtained with (**??**), and with the electromagnetic constitutive equation $\boldsymbol{P} = \boldsymbol{D} - \epsilon_0 \boldsymbol{E}$, in which ϵ_0 is the vacuum permittivity.

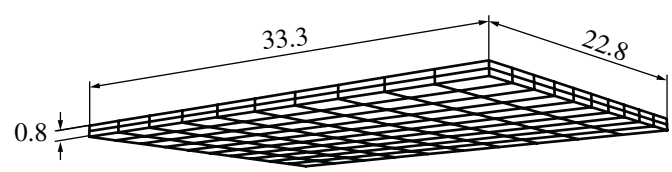

Fig. 4. Piezoelectric 7R-34-23-2500 manufactured by `Piezotite` [**?**], dimensions in (mm). Finite element mesh composed of 200 eight-node, three-dimensional isoparametric elements.

A. Actuator modeling

A typical spike signal depending on frequency ω is $V(t) = \exp(-\omega t)$: these signals are commonly used in biomedical applications [**?**]. The maximum voltage is approximately 840 (V), according to the manufacturer specifications. Consequently, a time-dependent electric field along the vertical direction with maximum value $E_z \approx -9 \times 10^5$ (V/m) is generated. Notice that the negative sign of E_z is due to the zero voltage at the bottom and the positive voltage at the top.

The generated polarization P_z (direct effect) through the thickness of the plate is represented versus the indirectly prescribed E_z in the Fig. **??** top. For τ_P = 0, the distribution should be a straight line since no dissipation is activated in the formulation. However, a non-zero τ_P induce hysteresis loops due to the Debye memory from (**??**) since from its integral, it is clear that the effective permittivity $\boldsymbol{\epsilon}$ depends on time.

Notice that the loops' inclination reduces with the increase of τ_P; the explanation can be found in the last (**??**): the higher the relaxation time the closer the exponential value to 1 and the derivative of $\boldsymbol{D}$ (proportional to P_z) with respect to the electrical field tends to zero.

In the bottom figure, the two generated P_z and S_{zz} are related. Both magnitudes are fully coupled through the piezoelectric effect and loops appear, but now due to the product of $\boldsymbol{e}^V$ with the exponential of (**??**). Because of this loop, a given

Property	Value	Units
C_{11} / C_{33} / C_{44} / C_{66} / C_{12} / C_{13}	143.7 / 129.8 / 29.41 / 29.41 / 82.7 / 82.3	$\times 10^9$ (N/m^2)
e_{31}^V / e_{33}^V / e_{15}^V	-7.35 / 13.61 / 11.76	(N/m·V)
ϵ_{11} / ϵ_{33}	8.49 / 7.76	$\times 10^{-9}$ (C/V·m]
ρ_m	7800	(kg/m^3)

TABLE I
MATERIAL PROPERTIES OF THE P-5E PIEZOELECTRIC OBTAINED FROM MANUFACTURER CATALOGUE, [**?**].

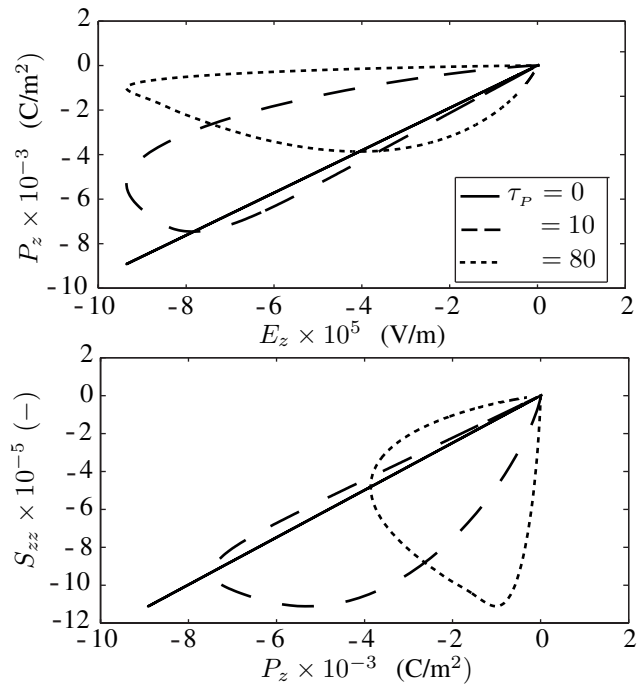

Fig. 5. Top: polarization generated by the applied electric field of Fig. **??** top (continuous line). Bottom: strain along thickness vs. generated polarization; three relaxation times in (s).

polarization causes two strain states depending on the time history. This "memory" behavior should be taken into account for the design of actuators, particularly in sophisticated applications that require the monitoring of precise deformations.

The inclination trend of the middle line is now the contrary to that of the previous figure; inspecting the before last (**??**), the reasoning of the exponential term still applies but the relative positions of the figure abscissa and ordinate have been exchanged.

As observed, the loop area increases with τ_P and, consequently, a frequency-dependency appears. This behavior is studied with detail in Fig. **??** for τ_P = 80 (s) and for three prescribed electric spikes with different frequencies. As in the previous figure, frequency-dependent polarizations (middle) and strains (bottom) are generated. From these results, it can be inferred that the loop areas decrease with frequency, trend consistent with the theoretical conclusions reported in [**?**] that states:

$$\boldsymbol{\epsilon} \quad \propto \quad \boldsymbol{\epsilon}^{\infty} + f\left(\frac{1}{\omega}\right), \tag{28}$$

where the symbol $\propto$ denotes "proportional to", f means "function of" and $\boldsymbol{\epsilon}^{\infty}$ is the permittivity in the absence of Debye memory. According to (**??**), an increase in frequency reduces the hysteresis-like second term of the right hand side, function of $1/\omega$.

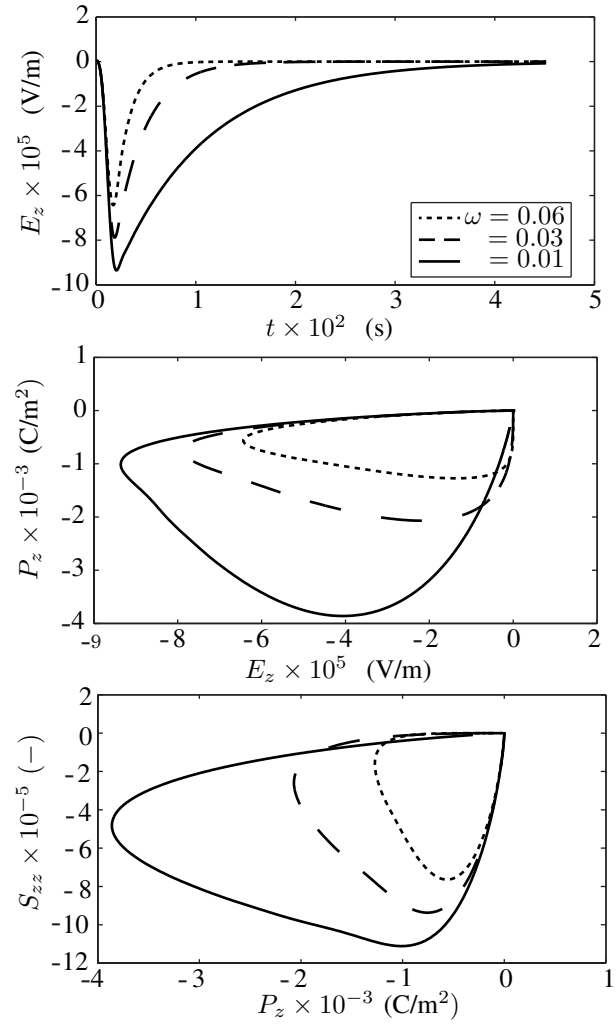

Fig. 6. Top: Prescribed electric field vs. time. Middle: polarization generated vs. applied electric field. Bottom: strain along thickness vs. generated polarization; three frequencies in (Hz) and relaxation time $\tau_P = 80$ (s).

From a numerical point of view, the stability of the time integration scheme, including Newmark-β and convolution integrals, is studied by representing the total energy of the system Π—the electromagnetic enthalpy (**??**)—versus time in Fig. **??**. Again, the three relaxation times are considered to compare results and the frequency is the minimum 0.01 (Hz).

All energies start at value zero, then they rapidly increases following the application of the electric pulse. After removal, the energy smoothly returns to zero and, therefore, it is demonstrated that the numerical integration is stable from the energetic point of view: spurious numerical energy is

not introduced in the system. For $\tau_P = 0$ the energy peak is approximately 8000 (J), for the others their maximum is smaller since the Debye memory introduces irreversibilities represented by Π^i in (**??**).

To qualify this effect and thermodynamically, the entropy balance is given by:

$$\rho_m \ \dot{s} = -\nabla \cdot \boldsymbol{j}_s + \sigma^s, \tag{29}$$

where s, $\boldsymbol{j}_s$ and σ^s denote entropy, entropy flux and entropy production, respectively. For reversible effects, $\sigma^s = 0$ and the entropy is conserved. But the Debye memory produces an entropy $\sigma^s = \dot{\boldsymbol{D}} \cdot \boldsymbol{E}/T$, where T is temperature in Kelvin scale. Therefore, part of the total electromechanical energy is converted into heat. Microscopically this heat is produced by the mentioned momentary delay of the dipoles.

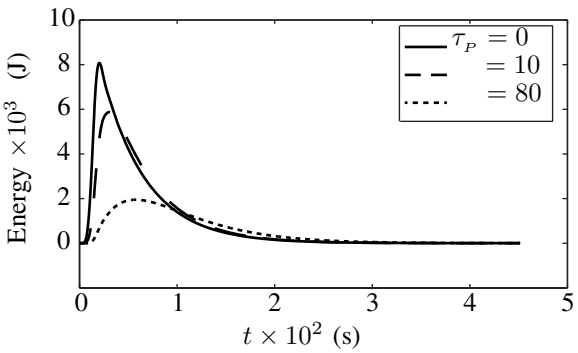

Fig. 7. Total electromagnetic enthalpy Π from (**??**) vs. time for three relaxations τ_P (s).

B. Sensor modeling

The other relevant application of piezoelectric devices is the sensor mode, which is simulated with results given in Fig. **??**: a sinusoidal mechanical vibration applied through the thickness of the piezoelectric plate is prescribed. Due to the piezoelectric coupling, polarization (top) and electric fields (bottom) are generated. Again, three relaxation times are assumed.

The most relevant observation is that the areas of the hysteresis loops are much smaller than those of the actuator situation from Fig. **??**. This fact is directly related with the frequency-dependency of the material properties. For instance, a one-dimensional (1D) analytical approximation of the strain and electric field generated during the actuator and sensor modes, respectively, can be estimated as functions of derivatives. In the top (**??**), $\boldsymbol{T} \approx \boldsymbol{0}$ since the plate is clamped in the complete lower face; from the bottom equation and since the only prescription is mechanical, $\boldsymbol{D}$ and its derivative is zero.

$$S_{zz} \approx f\left[\frac{e^V(\tau_P)}{C}\right] \frac{\partial V}{\partial z}, \qquad E_z \approx -f\left[\frac{e^V(\tau_P)}{\epsilon(\tau_P)}\right] \frac{\partial u}{\partial z}, \tag{30}$$

where C, $\epsilon(\tau_P)$ and $e^V(\tau_P)$ denote the 1D material properties. Notice that the last two coefficients decay with the inverse of τ_P, according to (**??**). As was observed in the previous subsection, in the actuator model the generated strain directly depends on ϵ. On the contrary, for the sensor mode the generated electric field depends of two frequency-dependent material properties: ϵ and e^V and, consequently, the memory effect is attenuated.

The loop areas slightly depend on τ_P as in Fig. **??**; in fact, the almost coincidence of all distributions can be explained by the simplification of the τ_P exponential term in (**??**). Again linear behavior is observed.

Finally, in this case the response is almost one-to-one: a given polarization value in the top figure produces the same strain since the memory effect is very weak, therefore, it is not necessary to considered the Debye memory to properly analyze electrical signals in this mode.

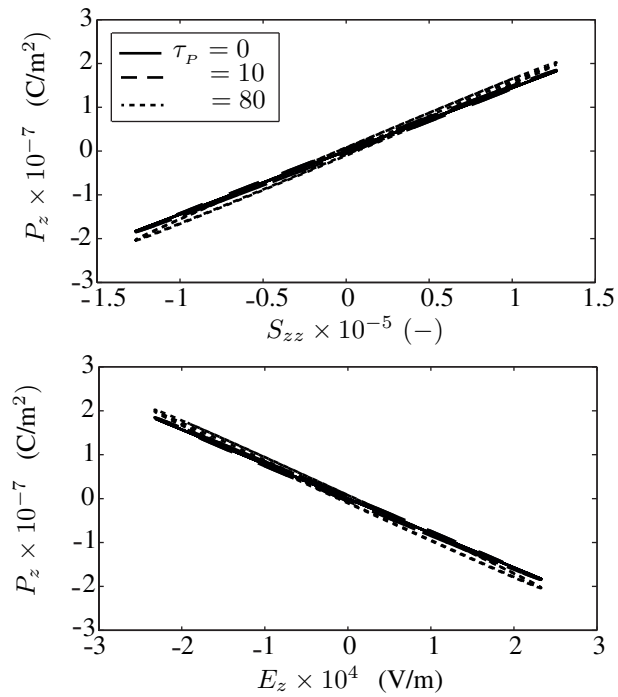

Fig. 8. Top: Generated polarization vs. prescribed strain $S_{zz} = \pm 1.25 \times 10^{-5} \sin 0.03t$ during 450 (s). Bottom: generated polarization vs. generated electric field. Three relaxation times τ_P in (s).

V. Conclusions

This work presents a numerical formulation within the finite element method to model piezoelectricity with Debye memory, which can be considered as a "viscosity-like" effect associated to the electric field through the inclusion of relaxation times. The formulation assumes material linearity and small strains and rotations.

Numerically, a monolithic formulation is developed, with its main difficulty arising from the time-dependency of the electrical constitutive equations. This difficulty is solved by using convolution integrals. Then, standard Newmark-β schemes are employed to solve the dynamics. Energy studies are conducted to guarantee the stability of the numerical time integration.

A commercial piezoelectric device for both actuator and sensor operation models is simulated and hysteretic-like behaviors are observed due to the electric memory. Obviously,

the hysteresis depends of the relaxation times and, consequently, a frequency-dependence appears. For the first model the loops are relevant, for the second they almost disappear.

Despite the fact that the Debye memory is not relevant in macro piezoelectric devices since the relaxation times are small, this effect could be relevant in novel and sophisticated micro- and nano-devices since the dimensions of the sample can be smaller than the intrinsic mean free path (a scale parameter in statistical physics) of the material. Also, this effect is relevant in high-speed applications such as ultrasonic propagations that are used in biological tissues.

The present numerical tool can be used for the design and optimization of more sophisticated mechatronic devices based on piezoelectric materials.

REFERENCES

[1] B. Zhang and Z. Zhu, Developing a linear piezomotor with nanometer resolution and high stiffness, *IEEE/ASME Transaction on Mechatronics*, 2(1), 22–29, 1997

[2] Y. Zhang, G. Liu and J. Hesselbach, On development of a rotatory-linear actuator using piezoelectric translators, *IEEE/ASME Transaction on Mechatronics*, 11(51), 647–650, 2006

[3] S. Wilcox and S. Devasia, Stability of velocity control for a piezoelectric stepper, *IEEE/ASME Transaction on Mechatronics*, 20(2), 910–923, 2015

[4] D. A. Berlincourt, D. R. Curran and H. Jaffe, Piezoelectric and piezomagnetic materials, *Physical Acoustic*, 1(A), 233–256, 1964

[5] R. Lerch, Simulation of piezoelectric devices by two and three dimensional finite elements, *IEEE Transactions on Ultrasonics, Ferroelectrics, and Frequency Control*, 37(2), 233–247, 1990

[6] J. L. Perez-Aparicio, H. Sosa and R. Palma, Numerical investigations of field-defect interactions in piezoelectric ceramics, *International Journal of Solids and Structures*, 44, 4892–4908, 2007

[7] R. Palma, G. Rus and R. Gallego, Probabilistic inverse problem and system uncertainties for damage detection in piezoelectrics, *Mechanics of Materials*, 41, 1000–1016, 2009

[8] G. Rus, R. Palma and J. L. Perez-Aparicio, Optimal measurement setup for damage detection in piezoelectric plates, *International Journal of Engineering Science*, 47, 554–572, 2009

[9] G. Rus, R. Palma and J. L. Perez-Aparicio, Experimental design of dynamic model-based damage identification in piezoelectric ceramics, *Mechanical System and Signal Processing*, 26, 268–293, 2012

[10] J. L. Perez-Aparicio, R. Palma and R. L. Taylor, Multiphysics and thermodynamic formulations for equilibrium and non-equilibrium interactions: non-linear finite elements applied to multi-coupled active materials, *Archives of Computational Methods in Engineering*, 23(3), 535–583, 2016

[11] A. J. Gil and R. Ortigosa, A new framework for large strain electromechanics based on convex multi-variable strain energies: Variational formulation and material characterisation, *Computer Methods in Applied Mechanics and Engineering*, 302, 293–3282, 2016

[12] A. Sáez, F. García-Sánchez and J. Domínguez, Hypersingular BEM for dynamic fracture in 2D piezoelectric solids, *Computer Methods in Applied Mechanics and Engineering*, 196, 235–246, 2006

[13] J. Debye, On the theory of anomalous dispersion in the region of long-wave electromagnetic radiation *(English Translation)*, *Verh. dtsch. phys. Ges.*, 15, 777–793, 1913

[14] B. Tiwari and R. N. P. Choudhary, Study of impedance parameters of cerium modified lead zirconate titanate ceramics, *IEEE Transactions on Dielectrics and Electrical Insulation*, 17(1), 5–17, 2010

[15] G. K. Zhu, M. Mojahedi and C. D. Sarris, Acoustic precursor wave propagation in viscoelastic media, *IEEE Transactions on Ultrasonics, Ferroelectrics, and Frequency control*, 61(3), 505–514, 2014

[16] D. Jou and G. Lebon, Extended Irreversible Thermodynamics, *Springer-Verlag Berlin Heidelberg*, 1996

[17] N. Newmark, A method of computation for structural dynamics, *J. Engr. Mech., ASCE*, 85, 67–94, 1959

[18] R. L. Taylor, FEAP A Finite Element Analysis Program: User Manual, *University of California, Berkeley*, 2010

[19] R. Palma, J. L. Perez-Aparicio, R. L. Taylor, Numerical formulation to study hysteresis behavior in magnetostrictive actuators, *IEEE/ASME Transaction on Mechatronics*, in progress, 2017

[20] J. R. Reitz and F. J. Milford, Foundations of Electromagnetic Theory, *Addison-Wesley Publishing Company, Inc.*, 1960

[21] S. R. de Groot and P. Mazur, Non-equilibrium Thermodynamics, *Dover*, 1984

[22] O. C. Zienkiewicz, R. L. Taylor and J. Z. Zhu, The Finite Element Method: Its basis and Fundamentals, 7th ed., *Elsevier Butterworth-Heinemann*, 2013

[23] R. D. Richtmyer and K. W. Morton, Difference methods for initial value problems, *Interscience*, 1967

[24] P. Gaudenzi and K. J. Bathe, An iterative finite element procedure for the analysis of piezoelectric continua, *Journal of Intelligent Material Systems and Structures*, 6, 266–273, 1995

[25] Piezotite, Murata Manufacturing Co, Ltd, *http://www.murata.com/*, 20170

[26] H. B. G. Casimir, Note on the Conduction of Heat in Crystals, *Physica*, 5(6), 495, 1938

[27] D. S. Dean, V. Démery, V. A. Parsegian and R. Podgornik, Out of equilibrium thermal Casimir effect in a model polarizable material, *Phys Rev E Stat Nonlin Soft Matter Phys.* , 85(3), 031108, 2012

[28] J. Melchor and G. Rus, Torsional ultrasonic transducer computational design optimization, *Ultrasonics*, 54(7), 1950–1962, 2014

[29] D. Damjanovic, Hysteresis in Piezoelectric and Ferroelectric Materials, *The Science of Hysteresis-Elsevier*, 3, 337–465, 2005

Roberto Palma received his Physics (2005), M. Sc. (2006) and Ph.D. degrees (2012) at the University of Granada (Spain). Currently, he is Assistant Professor at the Continuum Mechanics and Theory of Structures Department of the Universitat Jaume I (Spain). His research has gravitated around thermodynamic formulation for non-linear finite element applied to multi-coupled materials, optimization and inverse modeling, with some incursions in seismic engineering applied to experimental design in High Energy Physics.

José L. Pérez-Aparicio graduated (1983) as Mechanical Engineer at the Polythecnic Univ. Catalonia (Spain), as Master (1986) and as Ph.D. (1992) in Mechanical Engineer (minor in Aeronautics & Astronautics) at Stanford University (California). He has been professor at ICAI (Madrid), research professor at University of Granada and currently accredited full professor at Polythecnic University of Valencia. He has also taught at Drexel and Duke Universities. His research interest are related with numerical simulations on active materials, discrete methods and mechanical and aeronautical design.

Robert L. Taylor received his Ph.D. in 1963 in Civil Engineering from the University of California, Berkeley (UCB). He served as Professor until his retirement in 1994 and currently holds the title Professor of the Graduate School at UCB. His research interests are focussed mainly on problems in continuum mechanics with applications to solids, fluids and electro-mechanical devices. He is co-author of a three volume set of books related to finite element and related methods and is a member of the U.S. National Academy of Engineering.